Urban carbon dioxide cycles within the Salt Lake Valley: A multiple-box model validated by observations

C. Strong,[1] C. Stwertka,[1] D. R. Bowling,[2] B. B. Stephens,[3] and J. R. Ehleringer[2]

Received 24 January 2011; revised 20 April 2011; accepted 13 May 2011; published 11 August 2011.

[1] A multiple-box model was developed to determine how meteorological, anthropogenic, and biological processes combine to produce diel cycles of carbon dioxide (CO_2) mole fraction during each of the four calendar-based seasons within Salt Lake Valley, Utah, USA. The model was forced by observed winds, sounding-derived mixing depths, an anthropogenic CO_2 emissions inventory, and net biological flux estimates based on temperature, solar radiation, and ecosystem type. The model was validated using hourly CO_2 mole fractions measured at five sites in the urban Salt Lake Valley (uSLV) area for 2005–2009 (spatial average of observations denoted by C_{obs}). The model accounted for 53% of C_{obs} on an hourly basis, and accounted for 90–94% of the mean diel cycle of C_{obs} depending on season. The multiple-box model results indicated that CO_2 change rates within the uSLV mean diel cycles were largely the result of imbalances between anthropogenic processes adding CO_2 and meteorological processes removing or diluting CO_2. Removal by wind (advection) was the most important CO_2 reduction process on average, but dilution of CO_2 by entrainment of air from above the mixing height overtook advection in importance between sunrise and midday. During summer mornings, CO_2 reduction attributable to photosynthesis below shallow mixing heights was of intermediate importance between advection and entrainment, but the overall net effect of biological processes was the least important influence on CO_2 change rates during each of the four seasons.

Citation: Strong, C., C. Stwertka, D. R. Bowling, B. B. Stephens, and J. R. Ehleringer (2011), Urban carbon dioxide cycles within the Salt Lake Valley: A multiple-box model validated by observations, *J. Geophys. Res.*, *116*, D15307, doi:10.1029/2011JD015693.

1. Introduction

[2] Global atmospheric CO_2 is increasing and the decadal trends show no indication of a reduction in the rates of increase [*Intergovernmental Panel on Climate Change* (*IPCC*), 2007]. As global human populations become increasingly urbanized, spatially concentrated centers of anthropogenic CO_2 emissions emerge [*United Nations*, 2008; *Gurney et al.*, 2009; *Kennedy et al.*, 2009a]. At the same time, urban areas characteristically have CO_2 mole fractions and temperatures that are higher than global averages [*Idso et al.*, 2002; *Pataki et al.*, 2006a, 2006b; *George et al.*, 2007; *Pataki et al.*, 2007; *Kennedy et al.*, 2009a]. This pattern of localized CO_2 generation and dispersal results in urban CO_2 "domes" [*Idso et al.*, 2001, 2002; *Koerner and Klopatek*, 2002; *Pataki et al.*, 2007; *Andrews*, 2008]. As policy makers seek to explore ways in which to control or regulate carbon dioxide emissions, an increasing emphasis must be placed on understanding CO_2 sources and sinks in urban regions where much of the global increases in CO_2 are generated [*Gurney et al.*, 2009; *Kennedy et al.*, 2009b, 2009a; *Rosenzweig et al.*, 2010; *Wofsy et al.*, 2010a, 2010b].

[3] If CO_2 levels and or emissions are to be regulated, verification methods must be established. The Committee on Methods for Estimating Greenhouse Gas Emissions [*National Research Council*, 2010] has described the need for analytical and modeling tools that would allow for independent verification of CO_2 emissions at landscape, regional, and continental scales. Direct measurement of atmospheric CO_2 could provide a means for emission verification if urban atmospheric CO_2 can be distinguished from background concentrations and if meteorological processes influencing the dispersion of CO_2 emissions can be reconstructed. One of the scientific challenges is to understand the processes whereby background CO_2 levels are influenced by various CO_2 sources and sinks. Inversion models combining observation and processes have become a recent focus to address regional emissions patterns [*Ciais et al.*, 2010; *National Research Council*, 2010; *Reilly*, 2010; *Wofsy et al.*, 2010b; Z. Poussi et al., Carboscope: Greenhouse gases at the Earth's surface, 2010, available at http://www.carboscope.eu].

[4] The controls on CO_2 sources and sinks are dynamic and contrasting among different urban regions [*Grimmond*

[1]Department of Atmospheric Sciences, University of Utah, Salt Lake City, Utah, USA.
[2]Department of Biology, University of Utah, Salt Lake City, Utah, USA.
[3]National Center for Atmospheric Research, Boulder, Colorado, USA.

0148-0227/11/2011JD015693

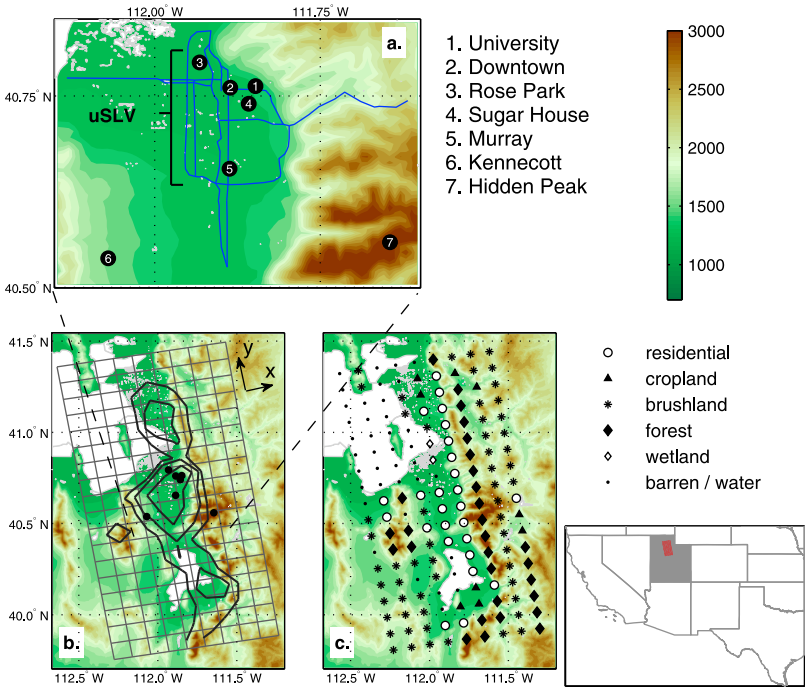

Figure 1. The map at the bottom right shows the southwestern United States with Utah shaded gray and the model domain shaded red. In Figures 1a–1c, shading indicates elevation in meters, and water is white with the Great Salt Lake toward the top left. (a) The Salt Lake Valley is shown. Blue curves are interstate highways, and numbered circles indicate measurement sites named to the right (sites 1–5 make up the urban Salt Lake Valley (uSLV)). (b) The region surrounding the Salt Lake Valley is shown with a grid indicating the edges of each 10 × 10 km model box, arrows indicating the model *x* direction and *y* direction, filled circles indicating the seven measurement sites in Figure 1a, and dashed lines indicating where the corners of Figure 1a align with Figure 1b. Annual mean anthropogenic CO_2 emissions are shown with units 10^{-7} kg m^{-2} s^{-1} at three contour levels: 0.25, 1, and 3. (c) The vegetation type assigned to each model box is indicated by a symbol as shown in the legend to the right.

et al., 2002, 2004; *Grimmond*, 2006; *Pataki et al.*, 2006a]. The urban forestry literature suggests that urban forests may contribute to an appreciable carbon sink [*Nowak and Crane*, 2002; *Nowak et al.*, 2002; *Gottschalk et al.*, 2010], yet the limited CO_2 flux literature shows that urban regions are net CO_2 sources to the atmosphere, with source strength sometimes diminished during vegetative summertime conditions [*Grimmond et al.*, 2004; *Moriwaki and Kanda*, 2004; *Ramamurthy and Pardyjak*, 2011]. Several studies have concluded that urban CO_2 fluxes strongly depend on variations in traffic and natural gas heating [*Nemitz et al.*, 2002; *Pataki et al.*, 2009], as well as factors such as land cover, climate, and season [*Ramamurthy and Pardyjak*, 2011, and references therein].

[5] The CO_2 mole fractions measured in cities evidence a sensitivity to factors that also influence CO_2 fluxes. Factors influencing the CO_2 mole fraction include proximity to urban centers and industrial sources, ground and air traffic, vegetation distribution, and rates of primary productivity [*Day et al.*, 2002; *Wentz et al.*, 2002; *Apadula et al.*, 2003; *Nasrallah et al.*, 2003; *Gratani and Varone*, 2005]. Advection patterns, atmospheric humidity, and topography also strongly impact CO_2 variability, evidencing a strong role for regional atmospheric processes [*Idso et al.*, 2002; *Moriwaki et al.*, 2006; *Ehleringer et al.*, 2008].

[6] Within the Salt Lake Valley (Utah, USA), near-surface CO_2 mole fractions have been measured continuously during the last decade using a network of infrared gas analyzers at urban and rural sites [*Pataki et al.*, 2003, 2006b; *Ehleringer et al.*, 2008, 2009] (Figure 1a and Table 1). Some of the network's CO_2 mole fraction records extend back to 2001 (http://co2.utah.edu), and evidence many of the sensitivities described above for urban settings. Salt Lake Valley CO_2 mole fractions are known to be strongly influenced by atmospheric stability and the height of capping inversions, and may be well-mixed horizontally during some persistent stable conditions [*Pataki et al.*, 2005; *Ehleringer et al.*, 2008]. Isotopic analyses of CO_2 at sites within the Salt Lake Valley have identified gasoline combustion as a year-round contributor to CO_2 variability, natural gas combustion as a major contributor during the winter months, and photosynthesis as a sink for CO_2 during the growing season [*Pataki et al.*, 2003, 2006b].

[7] A hierarchy of model complexities has been used to pursue various research questions concerning the variability of CO_2 fluxes and concentrations [*Enting*, 2002; *Ciais et al.*, 2010]. For the Salt Lake Valley, specifically, *Wofsy et al.* [2010b] have used the Salt Lake Valley CO_2 data with a high resolution transport model in an effort to calculate emissions based on observed mole fractions. *Reid and Steyn* [1997] used a multiple-box model and one month of data

Table 1. Description and Location of the Seven CO_2 Sampling Sites in the Salt Lake Valley Network[a]

Site	Measurement Height (m)	Latitude (°N)	Longitude (°W)	Elevation (masl)	Habitat
1. University	12	40.763	111.848	1,430	Residential with urban forest
2. Downtown	12	40.761	111.886	1,320	Multistory, commercial buildings with limited green space
3. Rose Park	6	40.794	111.932	1,299	Residential with limited urban forest development
4. Sugar House	6	40.740	111.858	1,339	Residential with mature urban forest development
5. Murray	6	40.655	111.887	1,325	Residential-commercial mix
6. Kennecott	9	40.538	112.070	1,580	Sagebrush steppe with adjacent dryland farming
7. Hidden Peak	18	40.561	111.645	3,350	Alpine with adjacent subalpine forest

[a]The number next to each site name is used to show the site location in Figure 1a.

from a CO_2 measurement site in Vancouver to understand the relative roles of meteorological, anthropogenic, and biological processes in determining local diel CO_2 cycles.

[8] Our aim in the present study is to quantify how meteorological, anthropogenic, and biological processes combine to produce the observed diel and seasonal cycles of CO_2 in the urban Salt Lake Valley (uSLV, Figure 1a) for all seasons. To accomplish this aim, we developed a computationally inexpensive multiple-box model framework inspired by *Reid and Steyn* [1997], and validated it using five years of observations from the Salt Lake Valley CO_2 network. The data and methods are described in section 2, seasonal and diel cycles are considered in section 3, and discussion is given in section 4.

2. Data and Methods

[9] Section 2.1 describes the CO_2 mole fraction observations. Sections 2.2 and 2.3 describe the multiple-box model and its boundary conditions. The methods used to prescribe the model's meteorological, biological, and anthropogenic input terms are described in sections 2.4–2.6. Model performance is discussed in section 2.7.

2.1. CO_2 Observations

[10] CO_2 mole fractions were measured at seven locations shown by filled circles in Figure 1a. Details for each site are given in Table 1. Measurements from five locations within the uSLV (sites 1–5, Figure 1a) were referenced to two baseline nonurban stations, one at the upper western edge of the Salt Lake Valley ("Kennecott"; site 6, Figure 1a) and one on an upper peak in the nearby Wasatch Mountains ("Hidden Peak"; site 7, Figure 1a). At sites 1–6, CO_2 concentration measurements were conducted using nondispersive infrared gas analyzers (IRGAs, LI-COR 7000 and LI-COR 6262; LI-COR, Lincoln, Neb.) coupled to dataloggers (CR23x; Campbell Scientific, Logan, Utah). Air was drawn into the building through tubing (Type 1300, Synflex Specialty Products, Mantua, Ohio), into a 5 liter glass buffer volume, through a magnesium perchlorate desiccant trap, and then through a solenoid system and flow controller before entering the IRGA. The pump was located downstream of the IRGA. The datalogger recorded 2 minute running averages every 5 minutes; these data were used to calculate hourly averages. Three World Meteorological Organization-traceable calibration standards were introduced into the gas analyzers every hour at Kennecott (site 6, Figure 1a) or 2–4 hours elsewhere to correct measurements to final values; the calibration tanks were coupled to the measurement system at the solenoid manifold. The Kennecott instrument was located outdoors, whereas the other instruments were located indoors. Hourly calibration of the Kennecott instrument was required to correct for temperature drift due to the high diel variability in temperature. The Hidden Peak (site 7) measurements were made using a single-cell IRGA (LI-COR 820), but with similar calibration gas frequencies [*Stephens et al.*, 2005].

[11] During 2005, we installed quality control cylinders at sites 1–6 to measure precision and accuracy of each system. Precision varied from 0.2 to 0.5 ppm CO_2, and accuracy from 0.03 to ±0.1 ppm CO_2 across the sites. As the ambient CO_2 values at these locations varied 2–60 ppm hourly, the accuracy and precision of the measurement systems were more than adequate to capture the natural temporal dynamics. All locations, except Kennecott, had Internet connections. Preliminary 5 minute data were posted online at http://co2.utah.edu for visual assessment (http://raccoon.ucar.edu for Hidden Peak). The Kennecott data were stored on the datalogger and downloaded at weekly intervals. Sites 1–6 were serviced at weekly intervals. Data were filtered to create a final data set with 1 hour averages. Filtering was used to eliminate erroneous data associated with various instrument problems, including empty calibration tanks, power failures, and clogged dessicant traps.

2.2. Multiple-Box Model

[12] As in the work of *Reid and Steyn* [1997], our model's basic formulation was a mass balance equation for CO_2 assuming diffusion was negligible [*Lettau*, 1970]

$$\frac{\partial(CA\,h)}{\partial t} = (Q_a + Q_b)A - u\frac{\partial(CA\,h)}{\partial x} - v\frac{\partial(CA\,h)}{\partial y} + HC_h\frac{\partial h}{\partial t}A \tag{1}$$

where C is CO_2 concentration, A is box horizontal area, h is box vertical extent ("mixing height"), Q_a is the anthropogenic CO_2 flux, Q_b is the net biological CO_2 flux, and C_h is the CO_2 concentration at h. The variables u and v are the horizontal components of wind in the model's x direction and y direction, respectively (grid orientation shown in Figure 1b). The term H represents the Heaviside step function with an argument $\partial h/\partial t$, which sets entrainment (last term on the right hand side) to zero if the mixing height is decreasing

$$H = \begin{cases} 1 & \text{if } \dfrac{\partial h}{\partial t} \geq 0 \\ 0 & \text{if } \dfrac{\partial h}{\partial t} < 0. \end{cases}$$

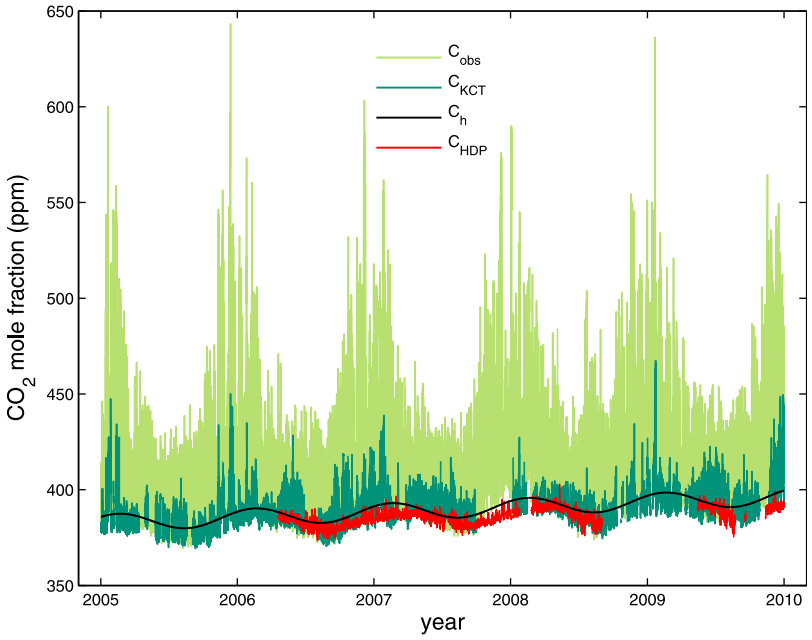

Figure 2. C_{obs} is hourly CO_2 mole fraction averaged across the five uSLV measurement sites (numbers 1–5 in Figure 1a), C_{KCT} is hourly CO_2 mole fraction measured at the rural "Kennecott" site (number 6 in Figure 1a), and C_{HDP} is hourly CO_2 mole fraction measured at the mountain "Hidden Peak" site (number 7 in Figure 1a). C_h is a smooth fit to C_{KCT}.

In (1), the units of concentration are kg m^{-3}, and the units of flux are kg m^{-2} s^{-1} with fluxes into the box being positive. For display and comparison to observations, we converted model CO_2 concentrations (kg m^{-3}) to CO_2 dry air mole fractions (ppm).

[13] The model boxes were arranged horizontally on a grid. Dividing by A and assuming h depends only on time, equation (1) can be written for box i as

$$\underbrace{\frac{\partial C_i}{\partial t}}_{\text{rate of change}} = \underbrace{\frac{Q_{a,i}}{h}}_{\text{anthropogenic}} + \underbrace{\frac{Q_{b,i}}{h}}_{\text{biological}} \underbrace{- u_i\left(\frac{\partial C}{\partial x}\right)_i - v_i\left(\frac{\partial C}{\partial y}\right)_i}_{\text{advection}} + \underbrace{\frac{H}{h}\frac{\partial h}{\partial t}(C_h - C_i)}_{\text{entrainment}} \quad (2)$$

where descriptive labels have been added to facilitate referring to terms in the equation.

[14] The model grid has $n_x = 9$ adjacent boxes in the east-west direction and $n_y = 18$ adjacent boxes in the north-south direction, for a total of 162 boxes (Figure 1b). For convenience, the placement of the 162 boxes on the map corresponded exactly to the 10 km grid on which the anthropogenic flux data were obtained (section 2.6). Domain boundaries (Figure 1b) were selected to capture the largest uSLV anthropogenic emissions, and to extend into regions where CO_2 mole fractions reduce to levels minimally affected by uSLV emissions. We integrated (2) using the Crank-Nicolson method [e.g., *Thomas*, 1995], meaning that terms on the right hand side were approximated by the average of their finite difference values at time j and $j + 1$. We used a 30 minute time step, and applied a 9-point selective optimized filter [*Bogey and Bailly*, 2004] at each time step for numerical stability.

2.3. Boundary Conditions

[15] We first describe how CO_2 concentrations at h (C_h) were specified, and then describe how lateral boundary concentrations were specified. Measurements of C_h were not available, so we objectively constructed a smooth C_h curve informed by available observations. We assumed that C_h had a magnitude lower than the average of the five uSLV sites (C_{obs}, Figure 2; sites 1–5 in Figure 1a) because CO_2 mole fractions generally decrease with increasing elevation in the absence of strong biological sinks [e.g., *Stephens et al.*, 2007], and mixing height h (section 2.4) generally ascended from ~100 m above the valley floor toward or beyond the elevation of the high-altitude Hidden Peak site (site 7 in Figure 1a and Table 1). We also assumed that C_h had magnitudes slightly higher than those observed at the Hidden Peak site (C_{HDP}, Figure 2) because convective daytime mixing above the urban valley floor did not always reach Hidden Peak [*de Wekker et al.*, 2009] and may have left elevated CO_2 mole fractions in residual layers that could be entrained during the ascent of the next morning's mixing height.

[16] We found that CO_2 mole fractions at the rural Kennecott site (C_{KCT}; site 6 in Figure 1a and Table 1) provided a useful base for constructing a C_h signal consistent with the above assumptions about magnitude, while also providing a trend and seasonal cycle similar to those observed at the high-altitude Hidden Peak site. The Kennecott site was distanced from concentrated urban emissions (Figure 1a), sparsely vegetated [*Ramamurthy and Pardyjak*, 2011], and

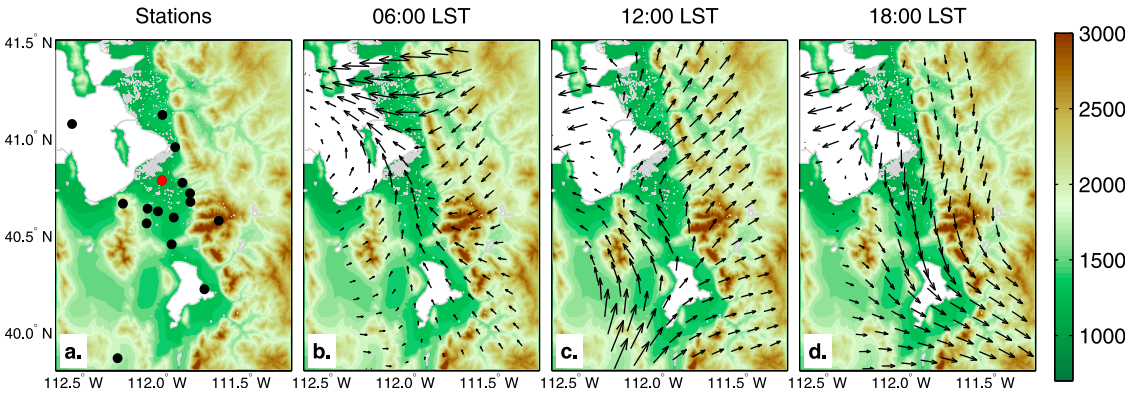

Figure 3. Shading indicates elevation in meters. (a) MesoWest wind data sites used in the study (filled black circles). Salt Lake City International Airport was also used (filled red circle). (b–d) Composite summer (JJA) surface wind fields for the times indicated. Each arrow corresponds to the center of one of the model boxes shown in Figure 1b, and the longest arrow represents a wind speed of 2.2 m s^{-1}.

situated at an elevation intermediate to the valley floor and Hidden Peak (Table 1).

[17] The formulation of our C_h curve was similar to *Thoning et al.* [1989]

$$C_h = a_1 t + a_2 \cos\left(\frac{2\pi t}{m}\right) + a_3 \sin\left(\frac{2\pi t}{m}\right) + a_4 \qquad (3)$$

where the first term represented the trend, the two trigonometric terms represented the seasonal cycle as a single harmonic with period m (one year), and the fourth term represented the mean. The parameters a_{1-4} were determined by performing a multiple linear regression of C_{KCT} on the right hand side of (3), and the resulting C_h curve is shown in Figure 2. The C_h curve averaged ~4 ppm higher than C_{HDP}, and was similar in shape to C_{HDP} (Figure 2). To further compare C_h and C_{HDP}, we fit C_{HDP} to (3); C_h led the C_{HDP} seasonal cycle by approximately one month, and C_h had a slightly larger trend (2.75 ppm per year compared to 2.29 ppm per year).

[18] We assumed that the effects of CO_2 advection above h from other major urban regions [e.g., *Levy et al.*, 1999] were negligible because the nearest major urban regions were hundreds of kilometers from our domain. Our choice of a smoothed seasonal cycle for C_h also neglected synoptic variability associated with arrival of air masses with anomalously high or low CO_2 mole fractions tied to interactions between weather and surface fluxes in areas around the model [e.g., *Parazoo et al.*, 2008]. Synoptic variability likely generated changes of several ppm in the actual value of C_h [e.g., *Keppel-Aleks et al.*, 2010], but modeling these variations without supporting measurements was beyond the scope of this study.

[19] Where and when the horizontal flow passed out of the domain, we used the so-called "upstream" method to calculate wave-permeable boundary conditions, meaning disturbances were allowed to leave the model domain with minimal boundary reflection [*Miller and Thorpe*, 1981; *Durran et al.*, 1993]. Where and when the horizontal flow was into the domain, our lateral boundary condition was the CO_2 concentration prescribed by C_h as formulated above, meaning we assumed that concentrations around the model domain were the same as those above the model domain.

2.4. Meteorological Fields

[20] Wind speed fields were developed using data from 16 measurement sites in the MesoWest data archive [*Horel et al.*, 2002]. Station locations (filled circles, Figure 3a) all had 10 m towers, and were chosen for representativeness, period of record, and data quality. Wind speed and direction were interpolated separately. We first assigned a wind speed to each model box center by fitting a smooth surface to the 16 wind measurements each hour. We then decomposed those interpolated wind speeds into eastward and northward components based on wind directions dictated by smooth surfaces fit to the 16 observed eastward and northward wind components each hour. The gridded hourly wind components were then converted to model x and y direction wind components (denoted here by u and v, respectively) using the angles between compass north and each grid point's y direction.

[21] Considering summer as an illustrative example, this wind specification procedure captured dominant topographical features of the local wind field [*Ludwig et al.*, 2004], including nocturnal drainage flow (Figure 3b) and the diel rotation of the flow along the valley axis (Figures 3b–3d). Composite diel cycles of v averaged over model boxes with uSLV measurement sites (sites 1–5 in Figure 1a) are shown for each season in Figures 4e–4h, further illustrating the characteristic shift from down-valley ($v > 0$) nocturnal flow to up-valley ($v < 0$) afternoon flow. The amplitude of this flow change was largest in summer (Figure 4g) and smallest in winter (Figure 4e).

[22] To estimate the mixing depth (h) during the daytime, we used the "parcel" method [*Holzworth*, 1967; *Miller*, 1967], meaning that h was set to the height at which the dry adiabatic lapse rate from each hourly surface air temperature intersected the profile of temperature recorded by the morning (12:00 GMT) radiosonde launched at the Salt Lake City International Airport (red filled circle, Figure 3a). At night, we used a constant value h = 100 m based on

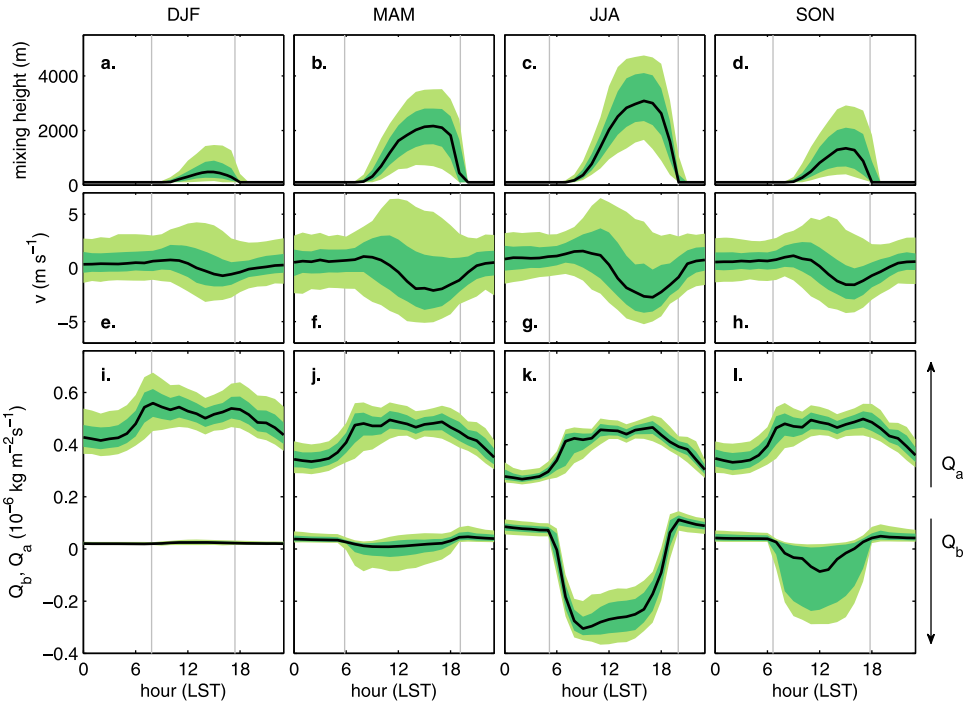

Figure 4. Composite diel cycles (local standard time) of model forcing averaged across model boxes containing uSLV measurement sites (numbers 1–5, Figure 1a), organized into columns by season: winter (DJF), spring (MAM), summer (JJA), and fall (SON). (a–d) Mixed layer height (h). (e–h) Wind component in model y direction (v). (i–l) Net anthropogenic flux (Q_a) appears as nonnegative curves in the top part of each plot, and net biological flux (Q_b) appears as curves crossing through zero in bottom part of each plot. For each variable, the bold curve is the median, the dark shaded region indicates the 25th to 75th percentiles, and the light shaded region extends to the 10th to 90th percentiles. Vertical lines indicate the time of sunrise and sunset in the middle of each 3 month window.

inspection of values for h obtained at sunrise (130–210 m depending on season).

[23] We experimented with more sophisticated models of h that involved determining stability classes, estimating turbulent heat fluxes, and distinguishing between mechanical and convective mixing [*Khan and Simpson*, 1997; *Seidel et al.*, 2010]. We found, however, that the deeper, mechanically induced mixed layer heights reduced CO_2 mole fractions unrealistically and generated relatively erratic changes in h that initiated numerical instabilities. Results presented here are thus based on the parcel method for daytime h. The composite mixing heights for each season (Figures 4a–4d) follow expected diel growth cycles, and maximal depths are in agreement with published climatological analyses [e.g., *Holzworth*, 1964].

2.5. Biological Fluxes

[24] To specify the net biological CO_2 flux (Q_b), we assigned each model box an ecosystem type (Figure 1c) based on United States Geological Survey (USGS) data originally collected in the 1970s and 1980s [*Price et al.*, 2006]. No attempt was made to adjust the ecosystem types for land use change after the USGS data collection period, but the extent of the urban forest was verified to align reasonably with the pattern of anthropogenic emissions (section 2.6; compare Figures 1b and 1c). Long-term measurements of Q_b were not available for the assigned ecosystems locally, so we identified a comparable "proxy" ecosystem in the AmeriFlux network (http://public.ornl.gov/ameriflux) for each local ecosystem (Table 2). Then, using at least four years of "level 4" AmeriFlux data from the

Table 2. The Vegetation Types Assigned to Model Boxes[a]

Vegetation Type	AmeriFlux Proxy	r^2	Scaling Factor
Brushland	Vaira Brushland V3 [*Xu and Baldocchi*, 2004]	0.80	1.0
Cropland	Mead Cropland V2 [*Verma et al.*, 2005]	0.79	1.0
Forest	Niwot Ridge V3 [*Monson et al.*, 2005]	0.54	1.0
Residential forest	Harvard Forest V2 [*Urbanski et al.*, 2007]	0.65	0.5
Wetland	Mead Cropland V2 [*Verma et al.*, 2005]	0.79	1.0

[a]Shown also are the proxy ecosystem data and version number in the AmeriFlux network used to develop the Q_b lookup table, the fraction of hourly variance in the proxy ecosystem accounted for by the lookup table based on a year of withheld data, and the scaling factor applied to the Q_b lookup table.

period 2001–2006, we developed a Q_b lookup table for each proxy ecosystem based on week of year, incoming solar radiation, and air temperature (Q_b is equivalent to net ecosystem exchange in the AmeriFlux data). Finally, to specify Q_b at each time step in a particular model box, we queried the corresponding proxy ecosystem Q_b lookup table with the conditions at the Salt Lake City International Airport: week of year, air temperature interpolated from hourly surface observations, and incoming solar radiation based on the solar angle and observed cloud fraction [*Holstag and Ulden*, 1983].

[25] Our analysis ignored the important role of water in ecosystem carbon fluxes in the interior West [*Anderson-Teixeira et al.*, 2011; *Bowling et al.*, 2010; *Hu et al.*, 2010]. For the irrigated urban forest, soil moisture was probably sufficient, but urban trees respond in a variety of ways to low humidity [*Bush et al.*, 2008]. Both soil moisture and humidity can be important environmental drivers of the surrounding native vegetation. Hence, our modeled biosphere contribution was probably larger than realistic. Our Q_b specification also assumed sufficient similarity between the proxy ecosystem and the local ecosystem in terms of factors including vegetation type, vegetation age, and vegetation density. A residential forest ecosystem was not available, so Harvard Forest was used as a proxy ecosystem for model boxes containing residential forest. Many of the urban tree species in the Salt Lake Valley are native to the temperate deciduous forests of New England. To adjust for the vegetation density difference between Harvard Forest and residential forest, the Harvard Forest–based Q_b lookup table was scaled by 0.5 (Table 2). The scaling value 0.5 is reasonable given the estimated canopy greenspace (percent tree cover divided by percent total greenspace) of Salt Lake City [*Nowak et al.*, 1996; *Nowak and Greenfield*, 2010], and the overall model performance was not sensitive to this parameter.

[26] Composite diel cycles of Q_b averaged across model boxes containing uSLV measurement sites (sites 1–5, Figure 1a) are shown for each season in the bottom half of Figures 4i–4l, and resemble well-documented patterns of variability at other sites [e.g., *Schmid et al.*, 2000]. Biological processes generally provided a net flux into the atmosphere during the night, and a net flux out of the atmosphere during the day. The amplitude of the diel biological flux cycle was largest in summer (Figure 4k) when daytime removal of CO_2 by the biosphere peaked.

2.6. Anthropogenic Fluxes

[27] Estimates of the anthropogenic CO_2 flux (Q_a) were developed from the "Vulcan" data set [*Gurney et al.*, 2009] of hourly fossil fuel emissions on a 10 km grid for the year 2002 (Figure 1b). The Vulcan data distinguished flux contributions from the following sectors: industrial, commercial, residential, on-road, nonroad, utility, aircraft, and cement. In using the Vulcan 2002 data, care was applied to address several issues: 1) the Vulcan day of week may not match the simulated day of week, meaning emissions due to traffic may not be representative, 2) 2002 air temperatures may not match 2005–2009 air temperatures, meaning emissions due to natural gas heating (which rival traffic in winter) may not be representative, and 3) the 2002 urban population count may not match the 2005–2009 population counts, meaning that total anthropogenic emissions may not be representative.

[28] To account for day of week effects, temperature effects, and population effects, our anthropogenic flux calculation for a given hour in model box i was

$$Q_{a,i} = \left(Q_{V,i} + \alpha_i e^{\beta_i T}\right)\gamma^{(Y-2002)} \quad (4)$$

where terms are as defined in the text below. $Q_{V,i}$ is the nonresidential portion of the Vulcan anthropogenic flux for the given hour in model box i taken from the nearest 2002 calendar date that matched the day of week being simulated. For example, to simulate Monday, 17 January 2005, we used the $Q_{V,i}$ values from Monday, 14 January 2002. The term with α_i and β_i is an empirical model of residential anthropogenic flux based on air temperature (T) at the Salt Lake City International Airport. The parameters α_i and β_i were fit for each model box separately using the hourly 2002 Vulcan residential flux and hourly values of T from 2002, and the r^2 for these fits ranged from 0.72 to 0.81 depending on model box. The constant $\gamma = 1.0163$ is a factor that accounts for the average annual rate of population increase for Salt Lake County (1.63% (U.S. Census Bureau, GCT-T1, Population estimates: Utah counties, 2000, available at http://www.census.gov)), and Y is calendar year.

[29] Annual mean values of Q_a are shown for the model domain in Figure 1b. Composite diel cycles of Q_a averaged over boxes containing uSLV measurement sites (sites 1–5, Figure 1a) are shown for each season in the top half of Figures 4i–4l, and contained traffic-driven peaks during the morning, near midday, and during the afternoon. The Q_a diel cycles exhibited this basic traffic-driven pattern in all seasons, but were shifted higher in the cooler months in part because of natural gas heating.

2.7. Model Performance

[30] Our primary aim for the model was to determine how meteorological, anthropogenic, and biological processes combine to produce diel cycles of CO_2 mole fraction during each of the four calendar-based seasons within the uSLV, where the uSLV is represented by measurement sites 1–5 in Figure 1a. The five uSLV sites were all in densely populated residential or commercial locations (Table 1) with major Interstate Highway traffic corridors nearby (curves, Figure 1a). Our 10 km multiple-box grid was not capable of resolving small-scale processes that generate different CO_2 mole fractions at the five uSLV sites in Figure 1a (one box in fact contains three uSLV sites), so we compared model output to CO_2 mole fractions averaged across the five uSLV sites (spatial average denoted C_{obs}).

[31] To calculate from the model output a quantity analogous to C_{obs} (denoted C_{mod}), we linearly interpolated the model output to the locations of the sensors that were used to calculate C_{obs}. If an observed value was not available for the calculation of C_{obs} during a particular hour, that site was excluded from the calculation of C_{mod} for the same hour. C_{obs} and C_{mod} were simple arithmetic means across the five station locations, and use of an area weighting scheme would have minimally impacted the results. Calculations of variance accounted for were based on squared Pearson

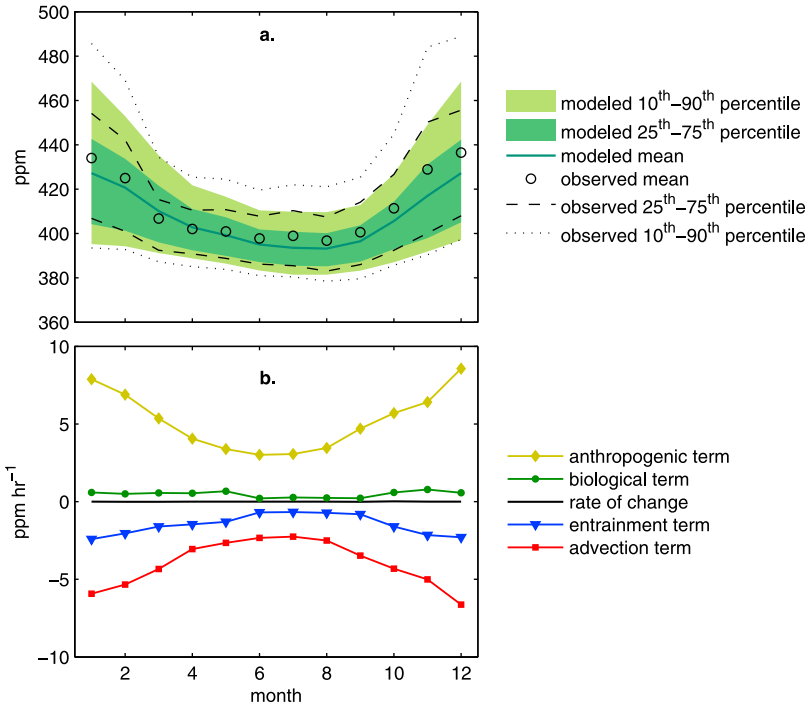

Figure 5. For the uSLV area: (a) Mean and percentiles of observed CO_2 mole fraction (C_{obs}) and modeled CO_2 mole fraction (C_{mod}) for each month of the year. (b) The monthly mean of terms in equation (2).

correlation coefficients (r^2). For hourly values from 2005–2009, C_{mod} accounted for 53% of C_{obs} with a mean bias error of −4.3 ppm and a mean absolute error of 13.5 ppm (statistical quantities defined by *Willmott and Matsuura* [2005]). C_{mod} accounted for 94% of the annual cycle constructed from monthly mean C_{obs} (statistic calculated for 12 pairs of numbers in Figure 5a), and accounted for 90 to 94% of the mean diel cycle of C_{obs} depending on season (statistics calculated for 24 pairs of numbers in Figures 6a–6d).

[32] The model results tended to underestimate C_{obs}, especially during colder months, as can be seen by comparing the mean and upper percentiles of C_{obs} and mean C_{mod} in Figure 5a. This low bias may result because the model assumed a uniform CO_2 mole fraction from the surface to height h, whereas CO_2 may in fact have been markedly elevated near the surface where C_{obs} measurements were made, particularly under stable conditions [e.g., *Moriwaki et al.*, 2006]. Agreement between C_{obs} and C_{mod} was better for the lower percentiles during each month (Figure 5a).

[33] We also evaluated model performance at the rural sites Kennecott and Hidden Peak (sites 6 and 7, respectively, Figure 1a). These sites were located approximately 200 to 2000 m above the uSLV sites (Table 1), so we disregarded cold season months when these sites may have resided above the model's mixing depth (December through February). At Kennecott, the model had a mean bias error of 4 ppm and accounted for approximately 75% of the variance in the mean diel cycle of CO_2. At Hidden Peak, the model had a mean bias error of 8 ppm, and accounted for approximately 30% of the variance in the mean diel cycle of CO_2. Detailed studies of variations at Hidden Peak [*de Wekker et al.*, 2009] evidence important roles for complex interactions between topography and the mixed layer that are not resolved by the multiple-box model.

3. Results

[34] We initialized the model with a uniform CO_2 field equal to C_h on 30 December 2004, and then ran the model through 31 December 2009. The 5 year simulation took less than 15 minutes to run on a desktop computer. Discarding the first 48 hours as an adjustment or "spin up" period, we present C_{obs} and C_{mod} results for the five complete years 2005–2009. Results focusing on the seasonal cycle are presented in section 3.1, and results focusing on diel cycle are presented in section 3.2.

3.1. Seasonal Variations

[35] Monthly mean C_{obs} achieved its annual maximum in December, and reached its annual minimum in July (circles, Figure 5). Monthly mean C_{mod} (solid curve, Figure 5) accounted for 94% of the variance of monthly mean C_{obs}. To determine how meteorological, anthropogenic, and biological processes combine to produce the CO_2 annual cycle, we averaged each of the labeled terms in equation (2) separately for each month across the model boxes containing the five uSLV measurement sites. Plots of these averages are shown in Figure 5b, serving as a measure of the relative importance of the various forcing terms and also as a measure of the model's sensitivity to forcing specification.

[36] In the monthly mean, the CO_2 rate of change term (Figure 5b) had very small deviations from zero that accounted for the shape of the seasonal cycle ("modeled mean" curve, Figure 5a), meaning the rate of change tended to be small and negative during the first half of the year (averaging -4.02×10^{-3} ppm hr^{-1}) and small and positive

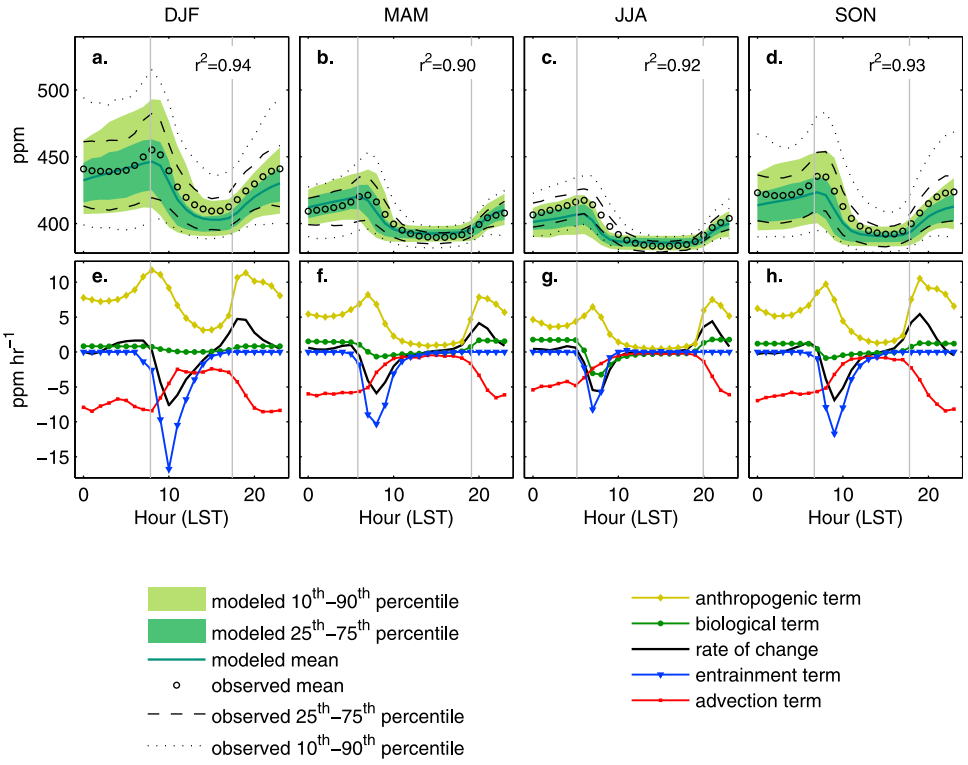

Figure 6. For the uSLV area: (a–d) Diel cycle of observed CO_2 mole fraction (C_{obs}) and modeled CO_2 mole fraction (C_{mod}) for season indicated at top (means and percentiles as shown in legend at bottom left). The squared Pearson correlation (r^2) between the observed and modeled mean diel cycle is indicated. (e–h) Mean hourly values of terms in equation (2) for the season indicated at top.

during the second half of the year (averaging 4.09×10^{-3} ppm hr^{-1}). Averaged over the entire simulation, the CO_2 rate of change term was slightly positive (3.20×10^{-5} ppm hr^{-1}) because of the upward trends in Q_a and C_h.

[37] In the monthly mean, the anthropogenic term was the largest factor (Figure 5b), and had its maximum values in the cold season when the mixing depth was shallow and emissions from natural gas heating supplemented emissions from traffic. The monthly mean biological term was positive but much smaller than the monthly mean anthropogenic term (Figure 5b). The near-zero magnitude of the monthly mean biological term resulted because the biological uptake (negative flux) was inversely correlated with the mixing depth over which it operated (compare Q_b in Figures 4i–4l to mixing depths in Figures 4a–4d), and was more than offset by respiration (positive flux) within shallower nocturnal mixing depths [*Denning et al.*, 1997]. Important nonzero values for the biological term at certain hours within the summer diel cycle are discussed in section 3.2. Wind ventilation (advection term, Figure 5b) and fresh air drawn in from above h during mixed layer growth (entrainment term, Figure 5b) offset nearly all the anthropogenic and biological flux into the atmosphere over the uSLV on a monthly mean basis. On average, advection accounted for approximately 3/4 of this offset.

3.2. Diel Variations

[38] The model captured the overall structure of the mean diel cycle of C_{obs} in each season (Figures 6a–6d), accounting for between 90 and 94% of its variance as indicated by the r^2 statistic at the top right of each plot. To determine how meteorological, anthropogenic, and biological processes combine to produce the observed diel cycles, we averaged each of the terms in equation (2) as in section 3.1, but now segregating data by season and hour of day (Figures 6e–6h). For all seasons, mean diel CO_2 mole fraction peaked close to sunrise (Figures 6a–6d) as emissions from rush hour traffic filled a shallow mixing depth with CO_2 (anthropogenic term, Figures 6e–6h). These peak morning mole fractions were kept in check by wind ventilation (advection curves, Figures 6e–6h), which offset approximately 70% of the anthropogenic surface fluxes on average throughout the day.

[39] Between sunrise and midday, rapid mixed layer growth diluted CO_2 mole fractions by drawing in fresh air from above h (entrainment term, Figures 6e–6h). Mixed layer growth also dampened the effect of anthropogenic fluxes by distributing them over a deepening mixed layer, as can be seen by comparing the shapes of the anthropogenic term (Q_a/h) curves in Figures 6e–6h to the anthropogenic flux (Q_a) curves in Figures 4i–4l. The mean diel CO_2 curves reached minimal values between midday and sunset (Figures 6a–6d) because maximum mixing depths (Figures 4i–4l) produced the greatest dampening of surface fluxes (e.g., afternoon depression in anthropogenic term, Figures 6e–6h). After sunset, CO_2 mole fractions increased (Figures 6a–6d) as emissions from traffic and cold season natural gas heating began to fill the shallow nighttime mixing depth.

[40] The rate of CO_2 dilution by mixed layer growth (entrainment term, equation (2)) was stronger in winter than during any other season (entrainment term curves, Figures 6e–6h). The strength of the winter entrainment term was principally due to large CO_2 concentrations (C_i) below the mixing height, and consequently large negative $C_h - C_i$ in equation (2). The large C_i values during winter resulted from anthropogenic CO_2 fluxes related to traffic and elevated natural gas heating (Figures 4i–4l) prior to the onset of daytime mixing. The total mixed layer growth during winter was small compared to other seasons (Figures 4i–4l), but the factor $h^{-1}\partial h/\partial t$ in the entrainment term (equation (2)) was comparable between seasons, confirming that interseasonal variations in entrainment were driven principally by $C_h - C_i$.

[41] The role of ecosystems was relatively small during all seasons except summer (biological term, Figure 6g). Warmer summer temperatures increased CO_2 release by soil respiration, and increased leaf area and solar radiation levels increased daytime CO_2 uptake by photosynthesis (Figures 4i–4l). During summer, active photosynthesis significantly contributed to CO_2 rates of decline in the relatively shallow mixed layer between sunrise and midday, and the resulting biological term magnitude was intermediate between advection and entrainment (Figure 6g).

4. Discussion

[42] A multiple-box model was developed to determine how meteorological, anthropogenic, and biological processes combine to produce diel cycles of carbon dioxide (CO_2) mole fraction within the urban Salt Lake Valley (uSLV) for all seasons. Model output was compared to CO_2 mole fractions spatially averaged across five measurement sites in the uSLV for 2005–2009 (C_{obs}). The model accounted for 53% of C_{obs} on an hourly basis, and accounted for 90–94% of the mean diel cycle of C_{obs} depending on season.

[43] During all four seasons, the mean diel cycle of C_{obs} peaked near sunrise, decreased rapidly between sunrise and midday, minimized in the afternoon, and then rose overnight. The multiple-box model results indicated that CO_2 mole fraction change rates within the uSLV diel cycles were largely the result of imbalances between anthropogenic processes adding CO_2 and meteorological processes removing or diluting CO_2. Anthropogenic fluxes, principally emissions from combustion of gasoline and natural gas, were the largest factor in the mass balance of uSLV CO_2. Advection was the most important CO_2 reduction process on average. During hours when surface temperatures were increasing, mixed layer growth reduced CO_2 mole fractions by entraining fresh air from above, and this dilution effect was generally stronger than advection between sunrise and midday. In addition, deepening of the mixed layer diluted the effects of surface fluxes, halving their effect from morning to afternoon during winter, and rendering surface fluxes nearly ineffectual during summer afternoons. Biological processes were the least important factor overall, except during summer mornings when photosynthesis within shallow mixing heights was of intermediate importance between advection and entrainment.

[44] Uncertainties in this study stem from assumptions or simplifications in the modeling framework, uncertainties in the input data sets, and the methods used to process input data. Estimates of model boundary conditions and understanding of model biases could be improved by more observations of CO_2 mole fraction spatial variability, particularly in the vertical dimension. Improvements to the estimates of C_h, informed by data collected above h, could be particularly important because most of the air volume in the mature mixed layer was entrained from above h. The model assumed a homogeneity of CO_2 mole fraction within each model box that may not be realistic, especially under stable conditions as discussed in section 2.7. The model also did not resolve topography, vertical variations in wind, or horizontal variations in mixing depth related to, for example, the urban heat island [*Khan and Simpson*, 2001]. The model's treatment of atmospheric processes was entirely observationally based. As such, the multiple-box model did not explicitly resolve flow complexities related to complex terrain, but it was computationally inexpensive and forced by flows and mixing depths that aligned with available observations.

[45] Although there are refinements to be incorporated into the next version of this modeling effort, it is clear that the current model captures the essential temporal features of the uSLV CO_2 cycle on diel and seasonal scales. The model thus provides a foundation appropriate for addressing the challenges laid out by the Committee on Methods for Estimating Greenhouse Emissions [*National Research Council*, 2010]. Consistent with findings reported by an earlier inversion study [*Pataki et al.*, 2007], the model results indicate that biological processes exert a prominent influence during certain hours, but are the least important factor overall in the uSLV. While reasons to plant trees may include carbon sequestration, shading, and esthetics, the model results do not support the notion that the carbon sink associated with the urban forest of the Salt Lake Valley largely offsets extensive emissions from fossil fuel combustion. The model results also indicate that fossil fuel emissions at levels consistent with Vulcan inventories [*Gurney et al.*, 2009] are required to account for the large diel cycle of urban CO_2 relative to background levels. Future model analyses can address projected consequences of changes in fossil fuel emissions associated with changes in human behavior, improved building efficiencies, urban planning, and/or biospheric sinks in a scenario fashion that can be useful for researchers and policy makers.

[46] The combined challenges of climate change through greenhouse gas forcing and expansion of urban systems are significant and require that more focus be placed on understanding the urban ecosystem carbon cycle dynamics. While international efforts are leading to a better understanding of the global carbon cycle [*IPCC*, 2007; *Ciais et al.*, 2010], regional efforts at the urban scale may prove more tractable in terms of evaluating the consequences of changes in human behavior on CO_2 emissions such as has been seen in integrated studies of fossil fuel consumption by *Pataki et al.* [2009]. Here it is clear that a greater emphasis on model development and testing with long-term data sets is required [*Reilly*, 2010; *Wofsy et al.*, 2010a]. The results of this current modeling study, when combined with the long-term spatial CO_2 monitoring and fossil fuel inventory data, provide a foundation for testing CO_2 emissions scenarios and human behavioral changes on a broad urban scale. Additional

modeling efforts by *Wofsy et al.* [2010b] should result in a series of model approaches that converge with this study toward a common objective: to provide the insights and data needed for policy makers when evaluating choices for carbon emission changes at the urban scale.

[47] Salt Lake City is a member of the C40 CITIES Climate Initiative (http://www.c40cities.org/), with efforts underway now to modify fossil fuel emission patterns in such a way that they might be detectable through long-term CO_2 observations and updated Vulcan inventories. With the proposed installation of a NEON site within the Salt Lake Valley (http://neoninc.org), there will be future opportunities to test refinements in our modeling effort at the urban and potentially suburban scales.

[48] **Acknowledgments.** Carolyn Stwertka was supported by a National Science Foundation (NSF) Think Globally, Learn Locally Fellowship (NSF award DGE08-41233). The Salt Lake Valley CO_2 observation network has been supported by the Office of Science (BER), U.S. Department of Energy, grants DE-FG02-06ER64309 and DESC0005266, and scientists who worked on the network include Andy Schauer, Andrew Moyes, Susan Bush, and Steve Rowley. The Hidden Peak measurements were supported NSF grant EAR-0321918 and National Oceanic and Atmospheric Administration grant NA09OAR4310064. The National Center for Atmospheric Research is sponsored by the NSF. We thank Dean Cardinale and the Snowbird Ski and Summer Resort for their support at the Hidden Peak site. The authors are grateful to John Horel for providing the Meso-West wind data, to Kevin Gurney for providing additional subsets of the 2002 Vulcan anthropogenic emissions data, to the Utah Division of Air Quality for guidance and data that informed treatment of anthropogenic emissions, and to principal investigators who provided AmeriFlux data to the archive at the Carbon Dioxide Information Analysis Center: Dennis Baldocchi, Russ Monson, Bill Munger, Shashi Verma, and Steve Wofsy. The authors thank three anonymous reviewers for comments that helped to improve the manuscript.

References

Anderson-Teixeira, K. J., J. P. Delong, A. M. Fox, D. A. Brese, and M. E. Litvak (2011), Differential responses of production and respiration to temperature and moisture drive the carbon balance across a climatic gradient in new mexico, *Global Change Biol.*, *17*, doi:10.1111/j.1365-2486.2010.02269.x.

Andrews, C. (2008), Greenhouse gas emissions along the rural to urban gradient, *J. Environ. Plann. Manage.*, *51*, 847–870.

Apadula, F., A. Gottia, A. Piginia, A. Longhettob, F. Rocchettia, C. Cassardob, S. Ferrareseb, and R. Forzab (2003), Localization of source and sink regions of carbon dioxide through the method of the synoptic air trajectory statistic, *Atmos. Environ.*, *37*, 3757–3770.

Bogey, C., and C. Bailly (2004), A family of low dispersive and low dissipative explicit schemes for flow and noise computations, *J. Comput. Phys.*, *194*, 194–214.

Bowling, D. R., S. Bethers-Marchetti, C. K. Lunch, E. E. Grote, and J. Belnap (2010), Carbon, water, and energy fluxes in a semiarid cold desert grassland during and following multiyear drought, *J. Geophys. Res.*, *115*, G04026, doi:10.1029/2010JG001322.

Bush, S., D. Pataki, K. Hultine, A. West, J. Sperry, and J. Ehleringer (2008), Wood anatomy constrains stomatal responses to atmospheric vapor pressure deficit in irrigated, urban trees, *Oecologia*, *156*, 13–20, doi:10.1007/s00442-008-0966-5.

Ciais, P., P. Rayner, F. Chevallier, P. Bousquet, M. Logna, P. Peylin, and M. Ramonet (2010), Atmospheric inversions for estimating CO_2 fluxes: Methods and perspectives, *Clim. Change*, *103*, 69–92.

Day, T. A., P. Gober, F. S. Xiong, and E. A. Wentz (2002), Temporal patterns in near-surface CO_2 concentrations over contrasting vegetation types in the Phoenix metropolitan area, *Agric. For. Meteorol.*, *110*, 229–245.

Denning, A. S., D. A. Randall, G. J. Collatz, and P. J. Sellers (1997), Simulations of terrestrial carbon metabolism and atmospheric CO_2 in a general circulation model, *Tellus, Ser. B*, *48*, 543–567.

de Wekker, S. F. J., A. Ameen, G. Song, B. B. Stephens, A. G. Hallar, and I. B. McCubbin (2009), A preliminary investigation of boundary layer effects on daytime atmospheric CO_2 concentrations at a mountaintop location in the Rocky Mountains, *Acta Geophys.*, *57*, 904–922.

Durran, D. R., M.-J. Yang, D. N. Slinn, and R. G. Brown (1993), Toward more accurate wave-permeable boundary conditions, *Mon. Weather Rev.*, *121*, 604–620.

Ehleringer, J., A. J. Schauer, C.-T. Lai, D. R. Bowling, D. E. Pataki, and B. B. Stephens (2008), Long-term carbon dioxide monitoring in Salt Lake City, *Eos Trans. AGU*, Fall Meet. Suppl., Abstract B43D-0466.

Ehleringer, J., A. Moyes, C. Cook, D. Pataki, C.-T. Lai, and A. Schauer (2009), Long-term results from an urban CO_2 monitoring network, *Eos Trans. AGU*, Fall Meet. Suppl., Abstract B33D-0414.

Enting, I. G. (2002), *Inverse Problems in Atmospehric Constituent Transport*, Cambridge University Press, Chicago, Ill.

George, K., L. Ziska, J. A. Bunce, and B. Quebedeaux (2007), Elevated CO_2 concentration and temperature across an urban-rural transect, *Atmos. Environ.*, *41*, doi:10.1016/j.atmosenv.2007.08.018.

Gottschalk, P., G. Churkina, M. Wattenbach, and U. Cubasch (2010), Assessment of the potential of urban organic carbon dynamics to off-set urban anthropogenic fluxes, *Eos Trans. AGU*, Fall Meet. Suppl., Abstract B21E-0355.

Gratani, L., and L. Varone (2005), Daily and seasonal variation of CO_2 in the city of Rome in relationship with the traffic volume, *Atmos. Environ.*, *39*, 2619–2624.

Grimmond, C. S. B. (2006), Progress in measuring and observing the urban atmosphere, *Theor. Appl. Climatol.*, *84*, 3–22.

Grimmond, C. S. B., T. S. King, F. D. Cropley, D. J. Nowak, and C. Souch (2002), Local-scale fluxes of carbon dioxide in urban environments: Methodological challenges and results from Chicago, *Environ. Pollut.*, *116*, S243–S254.

Grimmond, C. S. B., J. A. Salmond, T. R. Oke, B. Offerle, and A. Lemonsu (2004), Flux and turbulence measurements at a densely built-up site in Marseille: Heat, mass (water and carbon dioxide), and momentum, *J. Geophys. Res.*, *109*, D24101, doi:10.1029/2004JD004936.

Gurney, K. R., D. L. Mendoza, Y. Zhou, M. L. Fischer, C. C. Miller, S. Geethakumar, and S. de la Rue du Can (2009), High resolution fossil fuel combustion CO_2 emission fluxes for the United States, *Environ. Sci. Technol.*, *43*, 5535–5541.

Holstag, A. A. M., and A. P. V. Ulden (1983), A simple scheme for daytime estimates of surface fluxes from routine weather data, *J. Appl. Meteorol. Climatol.*, *22*, 517–529.

Holzworth, G. C. (1964), Estimates of mean maximum mixing depths in the contiguous United States, *Mon. Weather Rev.*, *92*, 235–242.

Holzworth, G. C. (1967), Mixing depths, wind speeds and air pollution potential for selected locations in the United States, *J. Appl. Meteorol.*, *6*, 1039–1044.

Horel, J., et al. (2002), Mesowest: Cooperative mesonets in the United States, *Bull. Am. Meteorol. Soc.*, *83*, 211–226.

Hu, J., D. J. P. Moore, S. P. Burns, and R. K. Monson (2010), Longer growing seasons lead to less carbon sequestration by a subalpine forest, *Global Change Biol.*, *16*, 771–783, doi:10.1111/j.1365-2486.2009.01967.x.

Idso, C. D., S. B. Idso, and J. R. C. Balling (2001), An intensive two-week study of an urban CO_2 dome in Phoenix, Arizona, USA Phoenix, AZ, USA, *Atmos. Environ.*, *35*, 995–1000.

Idso, S. B., C. D. Idso, and J. R. C. Balling (2002), Seasonal and diurnal variations of near-surface atmospheric CO_2 concentration within a residential sector of the urban CO_2 dome of Phoenix, AZ, USA, *Atmos. Environ.*, *36*, 1655–1660.

Intergovernmental Panel on Climate Change (IPCC) (2007), *Climate Change 2007: The Physical Science Basis: Working Group I Contribution to the Fourth Assessment Report of the IPCC*, edited by S. Solomon et al., Cambridge Univ. Press, New York.

Kennedy, C. A., et al. (2009a), Greenhouse gas emissions from global cities, *Environ. Sci. Technol.*, *43*, 7297–7302.

Kennedy, C. A., A. Ramaswami, S. Carney, and S. Dhakal (2009b), Greenhouse gas emission baselines for global cities and metropolitan regions, paper presented at Fifth Urban Research Symposium, World Bank, Marseille, France.

Keppel-Aleks, G., P. O. Wennberg, and T. Schneider (2010), Sources of variations in total column carbon dioxide, *Atmos. Chem. Phys. Discuss.*, *10*(12), 30,569–30,611, doi:10.5194/acpd-10-30569-2010.

Khan, S. M., and R. W. Simpson (1997), Modelling mixing height from routinely measured surface and upper air meteorological data, *Environ. Model. Assess.*, *2*, 191–200.

Khan, S. M., and R. W. Simpson (2001), Simulation of mixing depths incorporating the urban heat island effect, *Environ. Model. Assess.*, *6*, 183–193.

Koerner, B., and J. Klopatek (2002), Anthropogenic and natural CO_2 emission sources in an arid urban environment, *Environ. Pollut.*, *116*, S45–S51.

Lettau, H. H. (1970), Physical and meteorological basis for mathematical models of urban diffusion processes, in *Proceedings of Symposium on*

Multiple-Source Urban Diffusion Models, edited by A. C. Stern, U.S. Environ. Protect. Agency, Research Triangle Park, N. C.

Levy, P. E., A. Grelle, M. Molder, P. G. Jarvis, B. Kruijt, and J. B. Moncrieff (1999), Regional-scale CO_2 fluxes over central Sweden by a boundary layer budget method, *Agric. For. Meteorol.*, *98–99*, 169–180.

Ludwig, F. L., J. Horel, and C. D. Whiteman (2004), Using EOF analysis to identify important surface wind patterns in mountain valleys, *J. Appl. Meteorol. Clim.*, *43*, 969–983.

Miller, M. E. (1967), An atmospheric diffusion model for metropolitan areas, *J. Air Pollut. Control Assoc.*, *17*, 46–50.

Miller, M. J., and A. J. Thorpe (1981), Radiation conditions for the lateral boundaries of limited-area numerical models, *Q. J. R. Meteorol. Soc.*, *107*, 615–628.

Monson, R. K., J. P. Sparks, T. N. Rosenstiel, L. E. Scott-Denton, T. E. Huxman, P. C. Harley, A. A. Turnipseed, S. P. Burns, and B. Backlund (2005), Climatic influences on net ecosystem CO_2 exchange during the transition from wintertime carbon source to springtime carbon sink in a high-elevation, subalpine forest, *Oecologia*, *146*, 130–147.

Moriwaki, R., and M. Kanda (2004), Seasonal and diurnal fluxes of radiation, heat, water vapor and CO_2 over a suburban area, *J. Appl. Meteorol. Clim.*, *43*, 1700–1710.

Moriwaki, R., M. Kanda, and H. Nitta (2006), Carbon dioxide build-up within a suburban canopy layer in winter night, *Atmos. Environ.*, *40*, 1394–1407.

Nasrallah, H. A., J. R. C. Balling, S. M. Madi, and L. Al-Ansari (2003), Temporal variations in atmospheric CO_2 concentrations in Kuwait City, Kuwait with comparisons to Phoenix, Arizona, USA, *Environ. Pollut.*, *121*, 301–305.

National Research Council (2010), *Verifying Greenhouse Gas Emissions: Methods to Support International Climate Agreements*, Natl. Acad. Press, Washington, D. C.

Nemitz, E., K. J. Hargreaves, A. G. McDonald, J. R. Dorsey, and D. Fowler (2002), Micrometeorological measurements of the urban heat budget and CO_2 emissions on a city scale, *Environ. Sci. Technol.*, *36*, 3139–3146.

Nowak, D. J., and D. E. Crane (2002), Carbon storage and sequestration by urban trees in the USA, *Environ. Pollut.*, *116*, 381–389.

Nowak, D. J., and E. J. Greenfield (2010), Urban and community forests of the mountain region, *Tech. Rep. NRS-63*, U.S. For. Serv., U.S. Dep. of Agric., Newtown Square, Pa.

Nowak, D. J., R. A. Rowntree, E. G. McPherson, S. M. Sisinni, E. R. Kerkmann, and J. C. Stevens (1996), Measuring and analyzing urban tree cover, *Landscape Urban Plan.*, *36*, 49–57.

Nowak, D. J., J. C. Stevens, S. M. Sisinni, and C. J. Luley (2002), Effects of urban tree management and species selection on atmospheric carbon dioxide, *J. Aboriculture*, *28*, 113–122.

Parazoo, N. C., A. S. Denning, S. R. Kawa, K. D. Corbin, R. S. Lokupitiya, and I. T. Baker (2008), Mechanisms for synoptic variations of atmospheric CO_2 in North America, South America and Europe, *Atmos. Chem. Phys.*, *8*, 7329–7254.

Pataki, D. E., D. R. Bowling, and J. R. Ehleringer (2003), Seasonal cycle of carbon dioxide and its isotopic composition in an urban atmosphere: Anthropogenic and biogenic effects, *J. Geophys. Res.*, *108*(D23), 4735, doi:10.1029/2003JD003865.

Pataki, D. E., B. J. Tyler, R. E. Peterson, A. P. Nair, W. J. Steenburgh, and E. R. Pardyjak (2005), Can carbon dioxide be used as a tracer of urban atmospheric transport?, *J. Geophys. Res.*, *110*, D15102, doi:10.1029/2004JD005723.

Pataki, D. E., R. J. Alig, A. S. Fung, N. E. Golubiewski, C. A. Kennedy, E. G. McPherson, D. J. Nowak, R. V. Pouyat, and P. Romerolankao (2006a), Urban ecosystems and the North American carbon cycle, *Global Change Biol.*, *12*, 2092–2102, doi:10.1111/j.1365-2486.2006.01242.x.

Pataki, D. E., D. R. Bowling, J. R. Ehleringer, and J. M. Zobitz (2006b), High resolution atmospheric monitoring of urban carbon dioxide sources, *Geophys. Res. Lett.*, *33*, L03813, doi:10.1029/2005GL024822.

Pataki, D. E., T. Xu, Y. Q. Luo, and J. R. Ehleringer (2007), Inferring biogenic and anthropogenic carbon dioxide sources across an urban to rural gradient, *Oecologia*, *152*, 307–322.

Pataki, D. E., P. C. Emmi, C. B. Forster, J. I. Mills, E. R. Pardyjak, T. R. Peterson, J. D. Thompson, and E. Dudley-Murphy (2009), An integrated approach to improving fossil fuel emissions scenarios with urban ecosystem studies, *Ecol. Complexity*, *6*, 1–14, doi:10.1016/j.ecocom.2008.09.003.

Price, C. V., N. Nakagaki, K. J. Hitt, and R. C. Clawges (2006), Enhanced historical land-use and land-cover data sets of the U.S. Geological Survey, *U.S. Geol. Surv. Digital Data Ser. 240*. [Available at http://pubs.usgs.gov/ds/2006/240/.]

Ramamurthy, P., and E. R. Pardyjak (2011), Toward understanding the behavior of carbon dioxide and surface energy fluxes in the urbanized semi-arid Salt Lake Valley, Utah, USA, *Atmos. Environ.*, *45*, 73–84.

Reid, K. H., and D. G. Steyn (1997), Diurnal variations of boundary-layer carbon dioxide in a coastal city—Observations and comparison with model results, *Atmos. Environ.*, *31*, 3101–3114.

Reilly, J. M. (2010), Economic data and models in a greenhouse gas monitoring system, *Eos Trans. AGU*, Fall Meet. Suppl., Abstract GC41G-02.

Rosenzweig, C., W. Solecki, A. A. Hammer, and S. Mehrotra (2010), Cities lead the way in climate-change action, *Nature*, *467*, 909–911.

Schmid, P., C. S. B. Grimmond, F. D. Cropley, B. Offerle, and H.-B. Su (2000), Measurements of CO_2 and energy fluxes over a mixed hardwood forest in the mid-western United States, *Agric. For. Meteorol.*, *103*, 357–374.

Seidel, D. J., C. O. Ao, and K. Li (2010), Estimating climatological planetary boundary layer heights from radiosonde observations: Comparison of methods and uncertainty analysis, *J. Geophys. Res.*, *115*, D16113, doi:10.1029/2009JD013680.

Stephens, B. B., A. Watt, and G. Maclean (2005), An autonomous inexpensive robust CO_2 analyzer (AIRCOA), in *Report of the 13th WMO/IAEA Meeting of Experts on Carbon Dioxide Concentration and Related Tracers Measurement Techniques, Boulder, Colorado, USA, 19–22 September 2005*, pp. 111–115, World Meteorol. Organ., Geneva, Switzerland.

Stephens, B. B., et al. (2007), Weak northern and strong tropical land carbon uptake from vertical profiles of atmospheric CO_2, *Science*, *316*, 1732–1735.

Thomas, J. W. (1995), *Numerical Partial Differential Equations: Finite Difference Methods*, Springer-Verlag, New York.

Thoning, K. W., P. P. Tans, and W. D. Komhyr (1989), Atmospheric carbon dioxide at Mauna Loa Observatory: 2. Analysis of the NOAA GMCC Data, 1974–1985, *J. Geophys. Res.*, *94*, 8549–8565.

United Nations (2008), World Urbanization Prospects: The 2007 Revision. Highlights, *Tech. Rep. ESA/P/WP/205*, New York.

Urbanski, S., C. Barford, S. Wofsy, C. Kucharik, E. Pyle, J. Budney, K. McKain, D. Fitzjarrald, M. Czikowsky, and J. W. Munger (2007), Factors controlling CO_2 exchange on timescales from hourly to decadal at Harvard Forest, *J. Geophys. Res.*, *112*, G02020, doi:10.1029/2006JG000293.

Verma, S. B., et al. (2005), Annual carbon dioxide exchange in irrigated and rainfed maize-based agroecosystems, *Agric. For. Meteorol.*, *131*, 77–96.

Wentz, E. A., P. Gober, J. R. C. Balling, and T. A. Day (2002), Spatial patterns and determinants of winter atmospheric carbon dioxide concentrations in an urban environment, *Ann. Assoc. Am. Geogr.*, *92*, 15–28.

Willmott, C. J., and K. Matsuura (2005), Advantages of the mean absolute error (MAE) over the root mean square error (RMSE) in assessing average model performance, *Clim. Res.*, *30*, 79–82.

Wofsy, S. C., et al. (2010a), Measurement requirements for greenhouse gas concentrations in support of treaty monitoring and verification, *Eos Trans. AGU*, Fall Meet. Suppl., Abstract GC41G-04.

Wofsy, S. C., K. McKain, J. Eluszkiewicz, T. Nehrkorn, D. E. Pataki, and J. R. Ehleringer (2010b), An observational method for verifying trends in urban CO_2 emissions using continuous measurements and high resolution meteorology, *Eos Trans. AGU*, Fall Meet. Suppl., Abstract A13F-0280.

Xu, L. K., and D. D. Baldocchi (2004), Seasonal variation in carbon dioxide exchange over a Mediterranean grassland in California, *Agric. For. Meteorol.*, *123*, 79–96.

D. R. Bowling and J. R. Ehleringer, Department of Biology, University of Utah, 257 S. 1400 E., Salt Lake City, UT 84112-0840, USA.

B. B. Stephens, National Center for Atmospheric Research, 1850 Table Mesa Dr., Boulder, CO 80305, USA.

C. Strong and C. Stwertka, Department of Atmospheric Sciences, University of Utah, 135 S. 1460 E., Salt Lake City, UT 84112-0010, USA. (court.strong@utah.edu)